CHALMERS
UNIVERSITY OF TECHNOLOGY

Introducing the Rankine vortex method for drag reduction in wall-bounded turbulent flows at low Reynolds number through streamwise vortex

Downloaded from: https://research.chalmers.se, 2024-04-27 09:58 UTC

Citation for the original published paper (version of record):
Altintas, A. (2024). Introducing the Rankine vortex method for drag reduction in wall-bounded turbulent flows at low
Reynolds number through streamwise vortex manipulation. Physics of Fluids, 36(2).
http://dx.doi.org/10.1063/5.0184434

N.B. When citing this work, cite the original published paper.

research.chalmers.se offers the possibility of retrieving research publications produced at Chalmers University of Technology.
It covers all kind of research output: articles, dissertations, conference papers, reports etc. since 2004.
research.chalmers.se is administrated and maintained by Chalmers Library

(article starts on next page)

Physics of Fluids

RESEARCH ARTICLE | FEBRUARY 12 2024

Introducing the Rankine vortex method for drag reduction in wall-bounded turbulent flows at low Reynolds number through streamwise vortex manipulation

Atilla Altıntaş

Check for updates

Physics of Fluids 36, 025123 (2024)
https://doi.org/10.1063/5.0184434

View Online
Export Citation
CrossMark

28 February 2024 08:49:05

AIP Publishing

Physics of Fluids ARTICLE pubs.aip.org/aip/pof

Introducing the Rankine vortex method for drag reduction in wall-bounded turbulent flows at low Reynolds number through streamwise vortex manipulation

Cite as: Phys. Fluids **36**, 025123 (2024); doi: 10.1063/5.0184434
Submitted: 25 October 2023 · Accepted: 15 January 2024 ·
Published Online: 12 February 2024

View Online Export Citation CrossMark

Atilla Altıntaş[a)]

AFFILIATIONS

Division of Urban Mobility, Department of Architecture and Civil Engineering, Chalmers University of Technology, SE-412 96 Gothenburg, Sweden

[a)]Author to whom correspondence should be addressed: altintas@chalmers.se and altintascfd@gmail.com

ABSTRACT

It is well known that the near-wall streamwise vortices, together with the streaks, are the most important turbulent structures closely associated with drag reduction. Weakening or modifying the streamwise vortices are, thus, general approaches in near-wall turbulent control studies. In this study, a novel approach to manipulate the flow is introduced and applied to a turbulent channel flow in order to achieve drag reduction. The idea behind the "Rankine vortex method" is to generate a force based on the statistical and geometrical information of streamwise vortices. Direct numerical simulations of a turbulent channel flow at a frictional Reynolds number, Re_τ, of 180 (based on the driving pressure gradient and channel half-width) are performed. The force is applied in the vicinity of the lower wall of the channel, and the results are comparatively analyzed for the cases with and without force implemented. A drag reduction of 10% is achieved. The theoretical flow control approach presented, along with the associated analysis, has the potential to enhance our current understanding of flow control mechanisms through the manipulation of near-wall turbulence.

© 2024 Author(s). All article content, except where otherwise noted, is licensed under a Creative Commons Attribution (CC BY) license (http://creativecommons.org/licenses/by/4.0/). https://doi.org/10.1063/5.0184434

28 February 2024 08:49:05

I. INTRODUCTION AND BACKGROUND

Many studies have addressed the existence of large-scale (LS) and very-large-scale motions that have a significant effect on the wall turbulence at high Reynolds numbers.[1–3] Jiménez[1] has reported the existence of large eddies with streamwise lengths of the order of 10–20 boundary-layer thicknesses in the logarithmic region of wall-bounded flows. These large eddies involve mostly streamwise velocity fluctuations and contain most of the streamwise kinetic energy. Many subsequent studies have reported that log-law LS motions strongly influence near-wall turbulent structures.[4–9] In a recent study, the effect of the LS motions on the near-wall turbulence in a frictional Reynolds number of 550 was shown.[10]

It has been shown that the dominant structures of the near-wall region are the streamwise velocity streaks and the quasi-streamwise vortices.[11–14] Furthermore, it is shown that at lower frictional Reynolds numbers, the near-wall streamwise vortices are the single most important turbulent structure for drag reduction.[15] This is also supported by the observation that streamwise vortices have been found to be responsible for both *ejection* and *sweep* events of the bursting process.[16] During the bursting event, approximately 70% of total turbulence production occurs. Thus, weakening or modifying the streamwise vortices is a common approach in near-wall turbulent control studies.

As discussed earlier, the primary objective in flow control studies is to manipulate the near-wall streamwise vortices. While there is an abundance of statistical and theoretical information available for locating the mean streamwise vortex, to the best of the author's knowledge, no study has applied this information to generate a control force. In this study, statistical and geometrical information of vortices is employed to identify the mean vortex structure within a turbulent wall-bounded flow near the wall. These data serve a dual purpose: generating a control force and enhancing our comprehension of the flow control mechanism. We have extended the method proposed by Kim *et al.*[17] by carrying their calculations one step forward to quantify the strength of these mean vortex structures. The resulting force is

© Author(s) 2024

anticipated to manipulate streamwise vortex structures in the vicinity of the wall.

The direct numerical simulations (DNS) are performed for a turbulent channel flow at a frictional Reynolds number of 180 in which the force excitation is applied along the spanwise direction (based on geometrical information of the mean streamwise vortices) in order to investigate the potential for drag reduction. Instantaneous flow fields and various statistical characteristics are analyzed for both cases with and without the force applied.

The paper is organized as follows: First, the methodology that includes a detailed theory behind the Rankine vortex method (RVM) and derivation of the force is presented, followed by a detailed description of the numerical method. In Sec. II, the results are presented and discussed and some concluding remarks are given in the final section.

II. METHODOLOGY

A. Obtaining the force and governing equations

Streamwise vorticity carries information of the mean streamwise vortex: the local minimum represents the edge and the local maximum represents the center of the Rankine vortex structure [see Figs. 1(a) and 1(b)].[17] The superscript "+" sign indicates a nondimensional quantity scaled by u_τ and ν, friction velocity, and kinematic viscosity, respectively.

Assuming that the velocity distribution inside the vortex is similar to that of the Rankine vortex [see Fig. 1(b)], Kim *et al.*[17] suggest to estimate the strength of the Rankine vortex structures; for the spanwise velocity fluctuations, we can write

$$\left|\frac{\partial w}{\partial y}\right|_{wall} \approx \left|\frac{w_e}{y_e}\right| = \left|\frac{w_e}{y_c - y_e}\right|\frac{y_c - y_e}{y_e} = 3\left|\frac{w_e}{y_c - y_e}\right| \approx 3\left|\frac{\partial w}{\partial y}\right|_c. \quad (1)$$

Here, w_e is the spanwise velocity fluctuation at the edge of the mean vortex structure, y_e is the height of the edge location from the wall, and y_c is the center of the mean Rankine vortex structure [Fig. 1(b)]. Figure 1(a) estimates the strength of the mean vortex structures at the center as $0.13\frac{u_\tau^2}{\nu}$ [see peak at $y^+ = 20$ in Fig. 1(a)]. Since

$$|\omega_x|_c = \left|\left(\frac{\partial w}{\partial y}\right)_c - \left(\frac{\partial v}{\partial z}\right)_c\right| = 2\left|\frac{\partial w}{\partial y}\right|_c,$$

Equation (1) reads

$$\left|\frac{\partial w}{\partial y}\right|_{wall} \approx \frac{3}{2}\left|\omega_x\right|_c = \frac{3}{2}0.13\frac{u_\tau^2}{\nu} \approx 0.19\frac{u_\tau^2}{\nu},$$

therefore,

$$w_e = 0.19 y_e \frac{u_\tau^2}{\nu}. \quad (2)$$

Further analysis below defines a relation between the strength of the mean vortex and wall shear stress in the vicinity of the wall. At the wall, the velocity gradient is directly related to the friction velocity,

$$u_\tau^2 = \nu\left.\frac{\partial u}{\partial y}\right|_{wall}. \quad (3)$$

Substituting Eq. (3) in Eq. (2), we obtain

$$w_e = 0.19 y_e \left.\frac{\partial u}{\partial y}\right|_{wall}. \quad (4)$$

This value, w_e, represents the weighted strength of the force that will be generated.

Two-point correlations are very effective for understanding the structure of the flow. Pick two points along the x_1 axis, say x_1^A and x_1^C, and sample the fluctuating velocity in the x_1 direction. Then, the correlation of the velocity u_1' is given by

$$B_{uu}(\hat{x}_1) = \overline{u_1'(x_1)u_1'(x_1 - \hat{x}_1)}, \quad (5)$$

where $\hat{x}_1 = x_1^A - x_1^C$.

The two-point velocity correlations, $R_{vv}(\hat{z}^+)$, are utilized to obtain the approximate mean diameters of the Rankine vortex structures in the spanwise direction. $R_{vv}(\hat{z}^+)$ has a minimum at approximately $z = 0.15$ [Fig. 2(a)] at $y^+ = 10$, which is approximately $z^+ = 27$ for $Re_\tau = 180$, and giving an estimate of the mean diameter of the streamwise vortex.[17] For $Re_\tau = 550$, in Fig. 2(b), the $R_{vv}(\hat{z}^+)$ profile at $y^+ = 10$ exhibits the minimum at approximately $z = 0.05$, which corresponds to the same z^+ value (approximately $z^+ = 27$) as $Re_\tau = 180$. This suggests that the mean diameter of the streamwise vortex is independent of the Reynolds number. We denote the diameter of the streamwise vortex as z_{dia}^+ and let $\Delta = 2z_{dia}^+$ to indicate one period of the sine function, which is expected to coincide with the

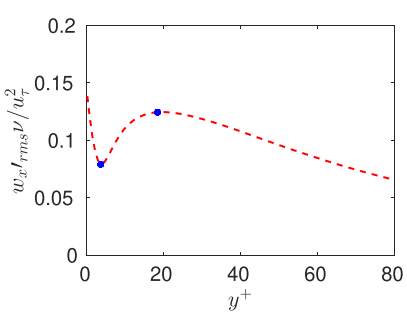

(a)Root mean square streamwise vorticity fluctuations. The maximum and minimum are indicated with a blue dot.

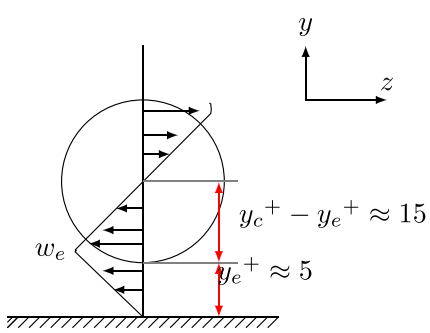

(b)Rankine vortex illustration.

FIG. 1. Streamwise vorticity fluctuations and Rankine vortex formation for $Re_\tau = 180$.

28 February 2024 08:49:05

© Author(s) 2024

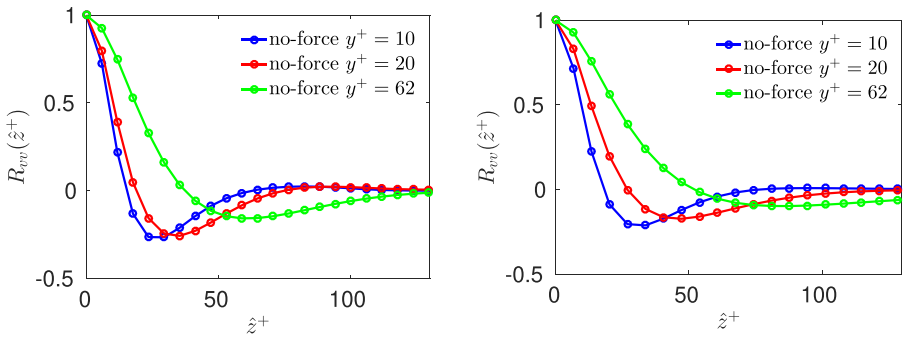

(a) $Re_\tau = 180$. (b) $Re_\tau = 550$.

FIG. 2. Wall-normal two-point velocity correlations.

vortex structures in the spanwise direction. Here, we define the RVM force as

$$F_z^+ = \pm w_e^+ (1 - (y^+ - y_e^+)^2/(y_c^+ - y_e^+)^2) \left| \sin\left(\frac{\pi}{\Delta} z^+\right) \right|. \quad (6)$$

Equation (6) is a time-independent spanwise body force. It has been applied both positive and negative to obtain a zero mean force in the spanwise direction (see Fig. 3).

The force part $(1 - (y^+ - y_e^+)^2/(y_c^+ - y_e^+)^2)$ is designed to regulate the force from the wall up to the center of the mean vortex. For example, at the edge of the vortex ($y = y_e$), where the spanwise velocity w_e is maximum [see Fig. 1(b)], the force part given above is equal to 1, resulting in the highest force at the edge. Conversely, at the center ($y = y_c$), where the spanwise velocity has its lowest value, the force part is equal to 0, leading to zero force. This ensures that the force generated aligns with the spanwise velocity distribution at the mean vortices from $y = y(0)$ up to the level of y_c.

It is essential to highlight that, contrary to the common practice of generating spanwise applied forces as oscillated sinusoidals to achieve a zero net force, the force introduced in this study does not exhibit sinusoidal periodicity. Although a component of the force includes the term $|\sin(\frac{\pi}{\Delta} z^+)|$, it is crucial to recognize that this term is consistently positive and lacks the characteristic alternating sign associated with periodic functions. Therefore, it does not induce any periodicity in the spanwise direction. Instead, to achieve a zero net force, the force is applied in both positive and negative directions.

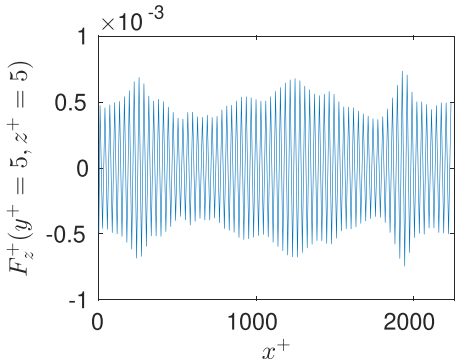

FIG. 3. Force along the streamwise direction. Force has zero mean in the spanwise direction.

Figure 4(a) illustrates the applied force in the wall-normal direction. A two-dimensional visualization is also depicted in Fig. 4(b). Force is applied to a level of $y^+ = 20$, which is the center of the mean vortex structure [see Fig. 1(b)].

B. Direct numerical simulations

The governing equations to solve in DNS for an incompressible Newtonian fluid are

$$\frac{\partial \mathbf{u}}{\partial t} + \mathbf{u} \cdot \nabla \mathbf{u} = \hat{\mathbf{e}}_1 \cdot \tilde{\mathbf{I}} - \frac{1}{\rho} \nabla p + \nu \nabla^2 \mathbf{u} + F_z, \quad (7)$$

$$\nabla \cdot \mathbf{u} = 0, \quad (8)$$

where a spanwise directed volume force, F_z, is added as a body force to the Navier–Stokes equations. Here, $\mathbf{u}$, p, and ρ are the velocity vector, the pressure, and the fluid density, respectively. The first term on the right-hand side of Eq. (7) is the driving force in the streamwise direction.

An implicit, two-step time-advancement finite volume method is used.[18] A central differencing scheme is used in space, and the Crank–Nicolson scheme is used in the time domain (see Altıntaş and Davidson[19] for further details).

A constant volumetric driving force is used in the streamwise momentum equation by which the frictional Reynolds number, $Re_\tau = 180$, is prescribed. Periodic boundary conditions are used in the streamwise and spanwise directions, while the usual no-slip boundary conditions are enforced at the walls. The domain size is $4\pi\delta \times 2\delta \times \pi\delta$ with grid sizes $148 \times 98 \times 98$, in the streamwise, wall-normal, and spanwise directions. The grid resolution is $\Delta x^+ \approx 15.$, $\Delta z^+ \approx 6$. A stretching of 1.065 is used in the wall-normal direction, which results in a minimum and maximum resolution as $\Delta y^+_{\min} \approx 0.16$, $\Delta y^+_{\max} \approx 2.88$.

The variables u, v, and w represent the streamwise, wall-normal, and spanwise velocities, respectively. Before applying any control, all simulations are allowed to reach a fully developed turbulent flow state. The results are, unless otherwise stated, averaged in all homogeneous directions (i.e., x_1, x_3, and t); the average is denoted by an overbar ($\bar{\cdot}$).

III. RESULTS AND DISCUSSION

DNS for turbulent channel flows are presented for analyzing the RVM efficiency. The force is applied to the lower (south) wall only. The drag history is shown in Fig. 5. Before a sudden and sharp decrease, an increase is observed on the drag for a short time at the

28 February 2024 08:49:05

© Author(s) 2024

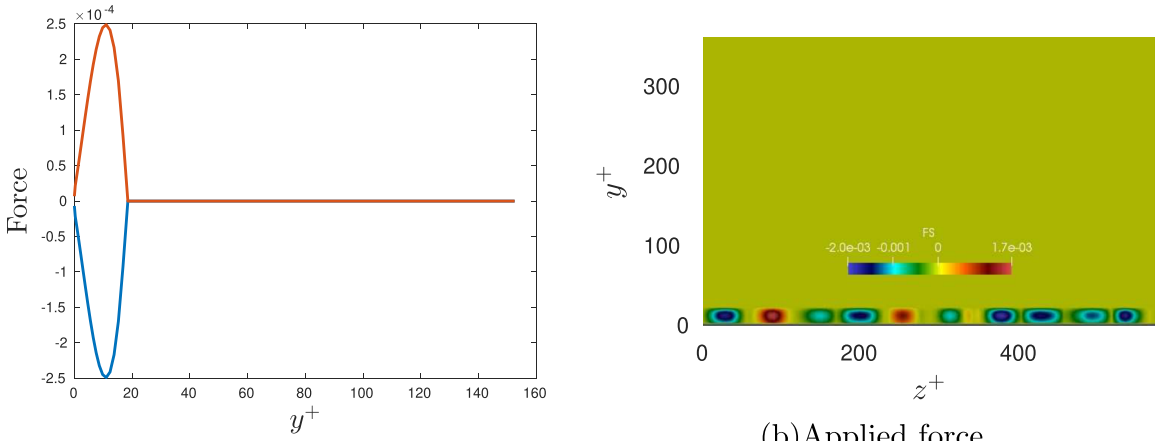

(a)Force characteristic in y^+ direction. (b)Applied force.

FIG. 4. Characteristics of the applied force at $Re_\tau = 180$.

beginning of the time histories. That could be due to the sudden high effect of the forcing on the velocities [see Figs. 6(b)–6(d)].

Figure 6(a) presents the mean velocity for the force and the no-force cases, compared with the DNS data.[20] In Fig. 6(a), for the applied force case, the viscous sublayer region intercepts with the log-law layer at a slightly higher y^+ level, and the higher shift of the intercept point is the result of the increase in the viscous sublayer thickness.[21] For u^+_{rms}, lower values are observed for the applied force case compared to the no-force case in the lower half of the channel [Fig. 6(b)]. For the applied force case, the wall-normal fluctuations exhibit a slightly higher value up to a level of $y^+ = 20$. Further away, it follows the no-force case up to half of the channel height. In the upper half of the channel, the force case gives higher values, compared to the no-force case [Fig. 6(c)]. As a result of the forcing, the spanwise rms velocity [Fig. 6(d)] exhibits a peak near the lower wall at around $y^+ = 20$, after that location it gradually decreases to the level of the no-force case at around $y^+ = 20$, and after that, it follows the no-force case for the rest of the channel.

Despite that the force is applied under the level of $y^+ = 20$, it significantly affects all three velocity components [Figs. 6(b)–6(d)] in the vicinity of the wall, is a sign of that near-wall turbulence structures have been highly manipulated. An estimation on the change of the

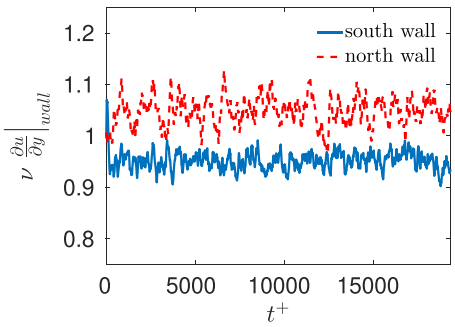

FIG. 5. Drag history.

vortex structures could be made by comparing Figs. 1(a) and 7(a). It has been shown before that spanwise oscillating Lorentz force modifies the mean vortex structure to a much smaller and elliptic shape.[19] Similarly, a closer distance between the streamwise rms vorticity minimum and maximum locations are also observed in the present study, which indicates that the mean vortex structure shrinks to a smaller form. The height of the edge location and the center of the mean vortex structure are modified from $y^+_e \approx 5$, $y^+_c \approx 20$ [see Fig. 1(b)], to $y^+_e \approx 8$, $y^+_c \approx 15$, for the applied force case. Therefore, the radius of the mean vortex structure is approximately two times lower for the applied force case compared to the no-force case. However, the strength of its center enhances approximately from $0.13\frac{u_\tau^2}{\nu}$ to a value of $0.28\frac{u_\tau^2}{\nu}$, which is about twice of that for the no-force case [Figs. 1(a) and 7(a)].

The shift in turbulence structures is evident through quadrant analysis, as illustrated in Fig. 7(b), which highlights the contributions to Reynolds shear stress from the second and fourth quadrants. Notably, when the force is applied, there is a noticeable displacement of sweep and ejection events away from the wall, as depicted in Fig. 7(b).

In the case of applied force, at the wall, sweeps exhibit a larger influence on the lower Reynolds shear stress up to a level of $y^+ \approx 25$. After this location, sweeps in the applied force case surpass the corresponding values in the no-force case. However, due to the increased contribution of ejections at that level, and the fact that the force case has lower values compared to the no-force case, a sustained lower Reynolds shear stress is maintained toward half of the channel height.

The results in Fig. 7(b) are in agreement with those in Fig. 7(a), suggesting that the edge of the mean vortex, y^+_e, shifts from $y^+_e = 5$ to $y^+_e = 8$. Together, Figs. 7(a) and 7(b) indicate that the applied force results in the relocation of vortex structures away from the wall. It is observed that for the applied force case the sweep events have a lower value up to a level of $y^+ \approx 20$ compared to the no-force case. Further away from the wall, it exhibits higher values compared to the no-force case. It is also observed that the ejection events are suppressed for the force case compared to the no-force case. For the applied force case,

28 February 2024 08:49:05

© Author(s) 2024

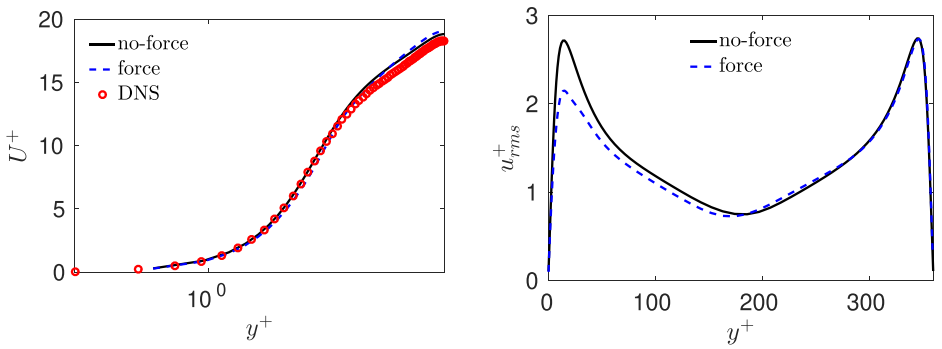

(a)Mean velocity. (b)Streamwise rms, u^+_{rms}.

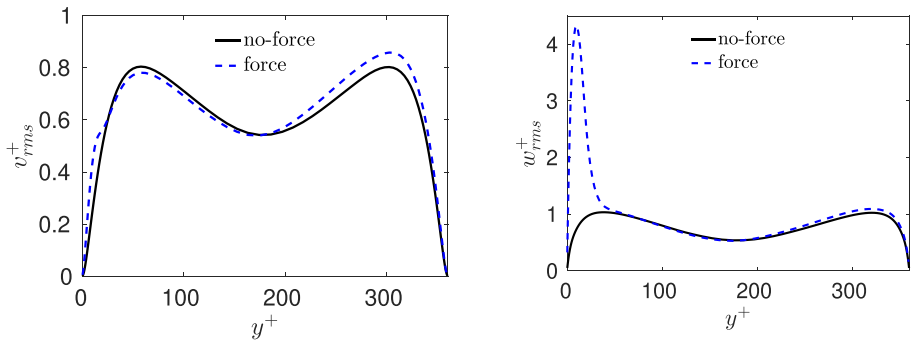

(c)Wall-normal rms, v^+_{rms}. (d)Spanwise rms, w^+_{rms}.

FIG. 6. Mean and fluctuation velocities. $Re_\tau = 180$.

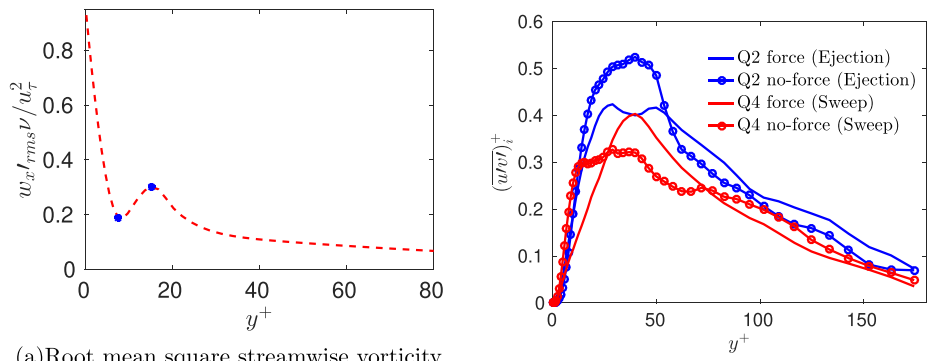

(a)Root mean square streamwise vorticity fluctuations, for the applied force case. The maximum and minimum are indicated with a blue dot.

(b)Quadrant analysis of sweep and ejections. Subscript i denotes the quadrant number, Q_i.

FIG. 7. Streamwise vorticity and quadrant analysis. $Re_\tau = 180$.

the ejection events have a lower value up to a level of $y^+ \approx 60$ compared to the no-force case. The applied force extends up to a threshold of $y^+ = 20$. Upon analyzing the results, it becomes evident that the force exerts a more pronounced influence below the wall-normal position of $y^+ \approx 50$, as illustrated in Fig. 6(d). Consequently, the ejection events appear to be suppressed, manifesting a primary peak at approximately $y^+ \approx 25$. Subsequently, these events exhibit a declining trend from this initial peak. However, with the mitigated impact of the force, there is a recovery leading to a secondary peak at around $y^+ \approx 55$. Beyond this threshold, a continuous descent is observed in the ejection events. Additionally, the absence of a secondary peak in the force case during the sweep event may be attributed to the phenomenon wherein sweeps progress toward the wall. This movement is characterized by decelerated motions succeeded by larger-scale connected motions directed toward the wall from above. These motions typically occur at small angles relative to the wall.[22]

The phenomenon known as the "streak cycle," which involves the regeneration of low-speed streaks and streamwise vortices, has been studied by Hamilton *et al.*[23] and Jiménez and Pinelli.[12] Their research demonstrated that this cycle is primarily driven by streak

28 February 2024 08:49:05

© Author(s) 2024

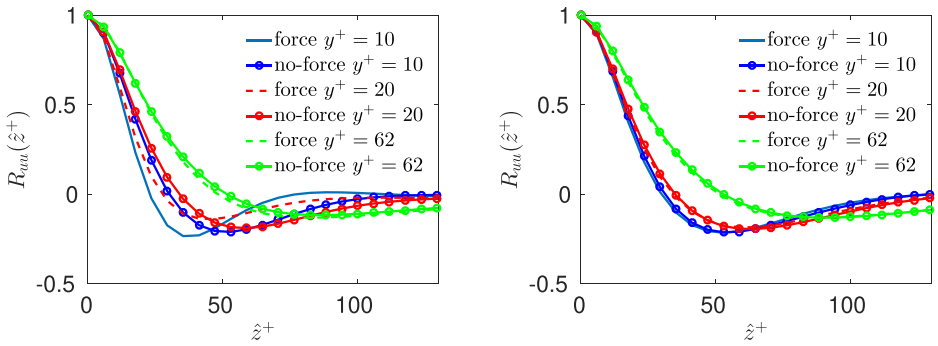

(a)Lower wall. (b)Upper wall.

FIG. 8. Streamwise two-point velocity correlations. $Re_\tau = 180$.

instability, leading to the formation of tilted streamwise vortices. These streamwise vortices, in turn, accumulate low-speed fluid and give rise to low-speed streaks. These streaks subsequently undergo wavy motions, ultimately resulting in streak instability.

In the present work, the forcing is directly targeting the vortex structures. Since the vortex structure is one of the two components of the streak cycle (streaks is the other), manipulating one will affect the other. Therefore, the modification of the vortex structures should modify the streaks. Streamwise velocity two-point correlation, $R_{uu}(\hat{z}^+)$, which carries information on the mean spacing between the streaks, is investigated to identify the effect of the modification of the vortex structures on streaky structures. The location of the minimum of the $R_{uu}(\hat{z}^+)$ provides an estimate of the mean separation between the high- and the low-speed fluid; the mean spacing between the streaks of high- and low-speed fluids is roughly twice that separation.[17] In Fig. 8, the streamwise velocity two-point correlations, $R_{uu}(\hat{z}^+)$, are shown near the lower and upper wall. The two-point correlation near the upper wall does not exhibit any modification [Fig. 8(b)]. In Fig. 8(a), we observe distinct characteristics in the correlations under the influence of force and in its absence. For the no-force case, the correlation reaches its minimum values at approximately $z^+ = 54$ for $y^+ = 10$, and $z^+ = 60$ for $y^+ = 20$, respectively. At $y^+ = 62$, the minimum occurs at $z^+ = 90$. In contrast, for the applied force case, the correlation exhibits minima at approximately $z^+ = 30$ for $y^+ = 10$ and $z^+ = 45$ for $y^+ = 20$. The shorter spacing between the high- and low-speed streaks indicates a deformation on the streaks. This is indicative of a reduced spanwise extent and deformation of the high- and low-speed streaks in the presence of force compared to the no-force case scenario.

The presence of a minimum in the spanwise velocity two-point correlation, $R_{ww}(\hat{z}^+)$, profiles (Fig. 9) was originally believed to be related to the separation of two streamwise vortices.[24] Later on, the cause of this minimum in $R_{ww}(\hat{z}^+)$ was modified to be impingement of high-speed fluid at the wall (splatting).[17,25] It has shown in Fig. 7(a) together with Fig. 7(b) that the turbulent structures shifted to a higher wall-normal location, which may explain why the splattings are not visible in the vicinity of the wall [Figs. 9(a) compared to 9(b)].

To further investigate in which way the forcing has modified the streaks, we refer to the instantaneous streamwise velocity contours (Fig. 10). Figures 10(a), 10(d), 10(g), 10(j), Figs. 10(b), 10(e), 10(h), 10(k), and Figs. 10(c), 10(f), 10(i), 10(l) represent the streamwise velocity contours for the no-force, the lower, and the upper wall for the applied force case, respectively. The contours from $y^+ = 10, 20$, and 30 clearly exhibit a reduction on the existency of the streaks, and both high- and low-velocity streaks appear in a much shorter and weaker form for the applied force case compared to the no-force case [Figs. 10(a), 10(b), 10(d), 10(e), 10(g), and 10(h)]. Compared to the lower wall, the upper wall exhibits streak formations similar to the no-force case [Figs. 10(c), 10(f), 10(i), and 10(l)]. At $y^+ = 62$, no-force and force for the lower and the upper wall exhibit similar velocity contours [Fig. 10(j) compared to Fig. 10(k)], which is in agreement with the two-point velocity correlations for the same y^+ location [see Figs. 8(a) and 9(a)].

In comparison with the force-applied case [Figs. 10(b), 10(e), 10(h), and 10(k)] with no force [Figs. 10(a), 10(d), 10(g), and 10(j)]

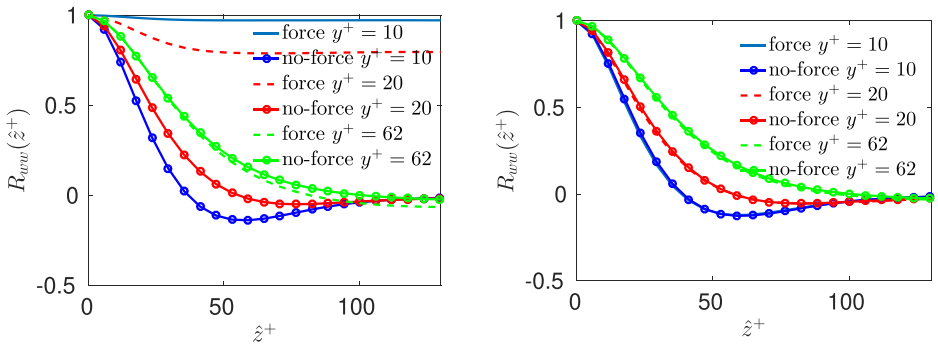

(a)Lower wall. (b)Upper wall.

FIG. 9. Spanwise two-point velocity correlations. $Re_\tau = 180$.

28 February 2024 08:49:05

© Author(s) 2024

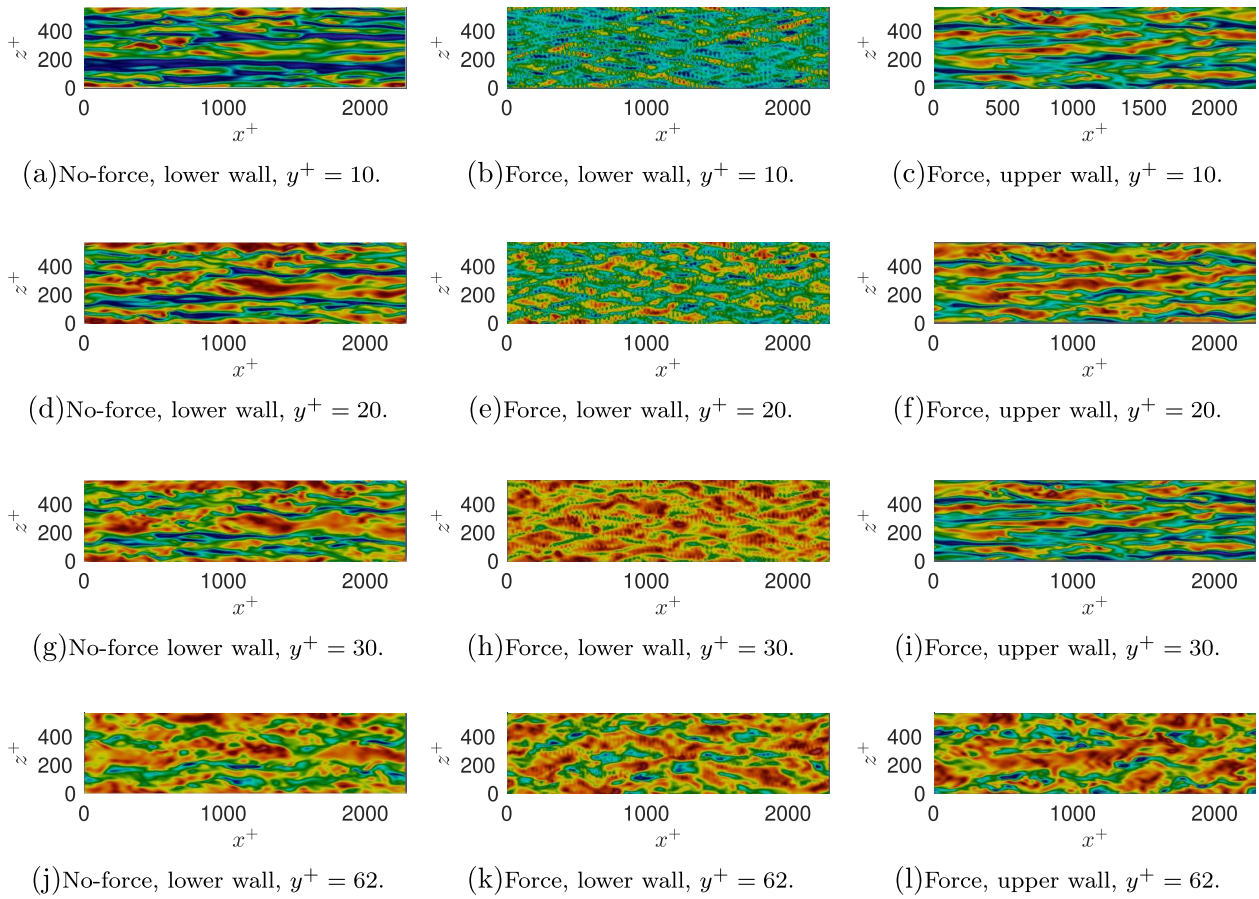

FIG. 10. Streamwise velocity (u) contours at the same instant for no-force lower, applied force lower and upper wall. Blue indicates low-speed streaks and yellow-red high-speed streaks. $Re_\tau = 180$. Contour levels range from 2.7 to 17, 5.9 to 19, 7.3 to 21, and 9.9 to 21, respectively, for $y^+ = 10$, 20, 30, and 62.

and the upper wall [Figs. 10(c), 10(f), 10(i), and 10(l)], two notable observations require explanation: the force-applied case exhibits much smaller streak formation, and high-velocity streaks dominate at higher wall-normal locations ($y^+ \geq 30$), i.e., low-velocity streaks are absent.

The diminished formation and absence of low-velocity streaks at higher locations may be attributed to the influence of the applied force on the bursting phenomena. The bursting process could be described by three stages: lifting of a low-speed streak from the wall, oscillation of gradually migrated low-speed streaks away from the wall, and the "breakup" of the streaks.[26] The breakup, the last stage of the bursting process, is also known as the beginning of the "cascade" processes that creates smaller fluctuations. In the second stage of bursting, also known as oscillatory growth motion, the dominant mode is streamwise vortices, in which vortex size grow and their strength increase.[26]

The answer to the former question, the smaller streak formation, is found in the comparison of Figs. 7(a) and 1(a), defining the strength of the mean vortex structure. Despite the modified vortices shrinking to a smaller form in the applied force case, their strength is approximately twice that of the no-force case. Consequently, it is concluded that in the second stage of the bursting process, where streamwise vortices dominate, strong vortices break the streaks before they attain a much longer form. This enhancement in streamwise vorticity and a proportional strengthening of near-wall vortices are also reported by Du *et al.*,[27] where drag reduction through spanwise traveling waves is investigated.

Quadrant analysis [Fig. 7(b)] suggest that in the force-applied case, ejections are altered, resulting in a reduction of bursting events, preventing the migration of low-speed velocities to higher locations. This is the reason that the dominant formation at higher levels ($y^+ \geq 30$) are high-speed streaks.

The normal vorticity, ω'_y, is a key indicator of formation of new streamwise vortices near the wall by streak instability.[28] The magnitude of ω'_y defines the level of the streaks' sinuous instability, i.e., streak waviness in the spanwise direction.[29] In Fig. 11(a), the streamwise rms vorticity, $\omega'_{y_{rms}}$, for the applied force case exhibits a reduction of about a factor of 1.1 compared to the no-force case.

Jeong *et al.*[30] related the spanwise fluctuation vorticity, $\omega'_{z_{rms}}$, with the existence of the low- and high-speed streaks. Figure 11(b) shows a comparison of the spanwise fluctuation vorticity, which indicates that the low- and high-speed streaks are reduced in the vicinity of the lower wall for the applied force case compared to the no-force case. The results are also in agreement with the streamwise velocity contours in

28 February 2024 08:49:05

© Author(s) 2024

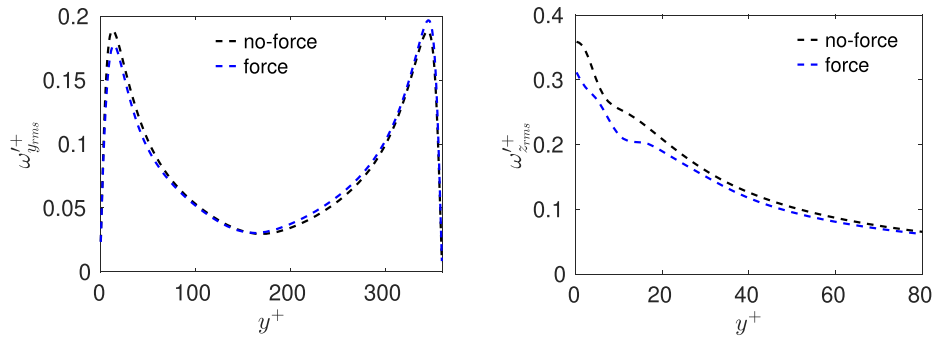

(a)Wall-normal fluctuation vorticity, $\omega'_{y_{rms}}$. (b)Spanwise fluctuation vorticity, $\omega'^{+}_{z_{rms}}$.

FIG. 11. Wall-normal fluctuation vorticity, $\omega'_{y_{rms}}$, and spanwise fluctuation vorticity, $\omega'^{+}_{z_{rms}}$. $Re_\tau = 180$.

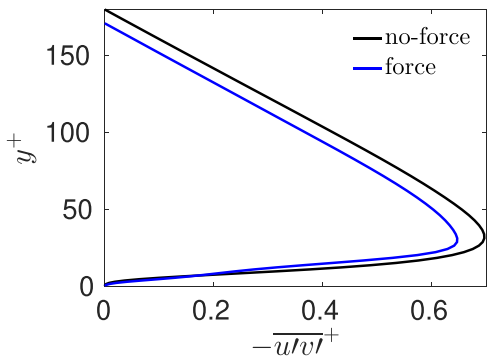

FIG. 12. Reynolds shear stress.

which a dramatical absence of the streak formation is observed (see Fig. 10).

The Reynolds shear stress and turbulence productions are presented in Figs. 12 and 13, respectively. The turbulence productions are compared with the DNS data of Lee and Moser.[20] As shown by Kim and Moin,[31] the vortical structures are associated with high Reynolds shear stress, $-\overline{u'v'}^+$, and it is observed here that a modification of the streamwise vortices and an absence of the related streaky structures result in lower Reynolds shear stress near the lower wall, as shown in Fig. 12. In alignment with the observed lower shear stress, turbulence production near the lower wall exhibits a noticeable reduction in the presence of the applied force [Fig. 13(a)]. In contrast, an equivalent degree of enhancement is observed near the upper wall as depicted in Fig. 13(b).

The term "Q-criterion" is derived from the second invariant of the velocity gradient tensor, as introduced by Hunt *et al.*[32] This second invariant, denoted as Q, is defined as

$$Q = \frac{1}{2}(\Omega_{ij}^2 - S_{ij}^2). \tag{9}$$

Here, the vorticity tensor is represented as $\Omega_{ij} = \frac{1}{2}(u_{i,j} - u_{j,i})$, and the strain rate tensor as $S_{ij} = \frac{1}{2}(u_{i,j} + u_{j,i})$. When Q isosurfaces are positive, it indicates that the strain rate tensor is smaller than the rotation tensor, effectively highlighting regions where rotation isolates strain. In other words, it provides a visual representation of vortices. A higher Q value corresponds to a more potent vortex.

The coherent vortices are analyzed using Q^+ values of 0.018 for cases with and without the applied force, as depicted in Figs. 14(a) and 14(b). In Fig. 14(a), which pertains to the no-force case, coherent structures are visible along both the lower and upper walls. Conversely, Fig. 14(b), representing the controlled wall with an applied force, illustrates a reduction in the size of the coherent structures.

The reduced size of mean vortex structure in the applied force case compared to the no-force case is evident in Fig. 7(a) in contrast to Fig. 1(a), where the local minimum and maximum define the edge, and the center of the mean vortex structure, respectively. The Q-criterion also supports these observations, clearly indicating that the applied force case exhibits a diminished size of vortices compared to the no-force case.

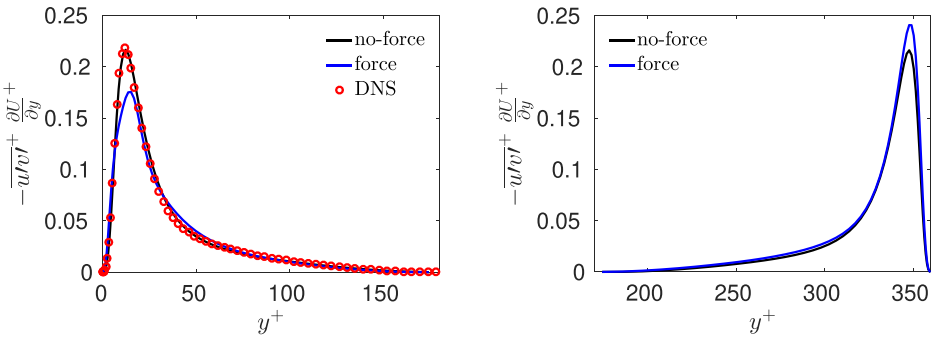

(a)Lower wall, $Re_\tau = 180$. (b)Upper wall, $Re_\tau = 180$.

FIG. 13. Turbulence production.

28 February 2024 08:49:05

© Author(s) 2024

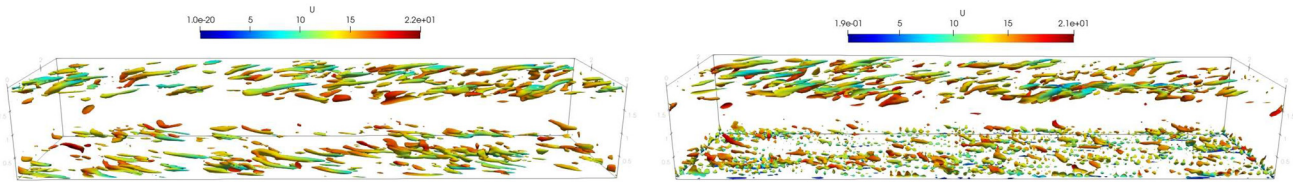

(a)No-force. (b)Force.

FIG. 14. Q-criterion. $Re_\tau = 180$. $Q^+ = Q/(u_\tau/\nu^2) = 0.018$.

IV. CONCLUSIONS

For the first time, geometrical information is directly used to generate a force that precisely targets the vortex structures. The theory targets the vortex structures result in a force that is a time-independent spanwise body force. The present forcing could explain the effectiveness of the spanwise forcing methods in general. That is supported by the analysis of the modified turbulent structures for the applied force case that exhibits similarities with the existing flow control studies using spanwise oscillated force.[11,19,27]

The mean vortex structure location is used as an estimation to locate the vortical structures. Of course, there exist vortex structures, which do not follow this pattern. It is noted that, however, the streak cycle is significantly affected by the applied force, but is not interrupted completely. The vortex structures still exist in the vicinity of the wall; otherwise, a full laminarization would be expected (see also Du *et al.*[27]).

We observe that the long formation of the streaks in the applied-force case is broken up to a much smaller formation compared to the no-force and applied-force cases [see Figs. 10(a), 10(d), 10(g), 10(j) and Figs. 10(b), 10(e), 10(h), 10(k)]. It is also shown that sinuous instability of the streaks is reduced by a factor of 1.1.

The application of the Q-criterion to our study has allowed us to scrutinize coherent vortices with Q^+ values set at 0.018 for cases with and without an applied force. Our findings, as depicted in Figs. 14(a) and 14(b), paint a compelling picture. In the absence of external force [Fig. 14(a)], coherent structures are clearly observable along both the lower and upper walls. However, in the presence of an applied force [Fig. 14(b)], a noticeable reduction in the size of these coherent structures becomes evident.

In summary, the present study represents a pioneering effort in the utilization of geometrical information to create a force precisely tailored to target vortex structures. This innovative theoretical approach yields a time-independent spanwise body force, in line with our expectations. Consequently, our examination of the altered turbulent structures in the presence of applied force closely aligns with established flow control studies that utilize spanwise oscillated force techniques, providing insights into the overall efficacy of spanwise forcing methods.

AUTHOR DECLARATIONS

Conflict of Interest

The authors have no conflicts to disclose.

Author Contributions

Atilla Altıntaş: Formal analysis (equal); Investigation (equal); Methodology (equal); Validation (equal); Writing – original draft (equal); Writing – review & editing (equal).

DATA AVAILABILITY

The data that support the findings of this study are available from the corresponding author upon reasonable request.

REFERENCES

[1] J. Jiménez, *The Largest Scales of Turbulent Wall Flows* (Center for Turbulence Research Annual Research Briefs, Stanford University, 1998).
[2] R. J. Adrian, C. D. Meinhart, and C. D. Tomkins, "Vortex organization in the outer region of the turbulent boundary layer," J. Fluid Mech. **422**, 1–54 (2000).
[3] J. Jiménez, J. C. Del Alamo, and O. Flores, "The large-scale dynamics of near-wall turbulence," J. Fluid Mech. **505**, 179–199 (2004).
[4] N. Hutchins and I. Marusic, "Evidence of very long meandering features in the logarithmic region of turbulent boundary layers," J. Fluid Mech. **579**, 1–28 (2007).
[5] R. Mathis, N. Hutchins, and I. Marusic, "Large-scale amplitude modulation of the small-scale structures in turbulent boundary layers," J. Fluid Mech. **628**, 311–337 (2009).
[6] P. Schlatter and R. Örlü, "Quantifying the interaction between large and small scales in wall-bounded turbulent flows: A note of caution," Phys. Fluids **22**, 051704 (2010).
[7] R. Mathis, I. Marusic, N. Hutchins, and K. Sreenivasan, "The relationship between the velocity skewness and the amplitude modulation of the small scale by the large scale in turbulent boundary layers," Phys. Fluids **23**, 121702 (2011).
[8] B. Ganapathisubramani, N. Hutchins, J. Monty, D. Chung, and I. Marusic, "Amplitude and frequency modulation in wall turbulence," J. Fluid Mech. **712**, 61–91 (2012).
[9] L. Agostini and M. Leschziner, "On the departure of near-wall turbulence from the quasi-steady state," J. Fluid Mech. **871**, R1 (2019).
[10] A. Altıntaş, L. Davidson, and S. Peng, "A new approximation to modulation-effect analysis based on empirical mode decomposition," Phys. Fluids **31**, 025117 (2019).
[11] T. W. Berger, J. Kim, and C. Lee, "Turbulent boundary layer control utilizing the Lorentz force," Phys. Fluids **12**, 631–649 (2000).
[12] J. Jiménez and A. Pinelli, "The autonomous cycle of near-wall turbulence," J. Fluid Mech. **389**, 335–359 (1999).
[13] S. J. Kline, W. C. Reynolds, F. A. Schraub, and P. W. Runstadler, "The structure of turbulent boundary layers," J. Fluid Mech. **30**, 741–773 (1967).
[14] J. Kim, "Physics and control of wall turbulence for drag reduction," Philos. Trans. R. Soc., A **369**, 1396–1411 (2011).
[15] J. Kim, "Study of turbulence structure through numerical simulations: The perspective of drag reduction," Technical Report, AGARD Report, 1992.
[16] S. K. Robinson, "Coherent motions in the turbulent boundary layer," Annu. Rev. Fluid Mech. **23**, 601–639 (1991).
[17] J. Kim, P. Moin, and R. Moser, "Turbulence statistics in fully developed channel flow at low Reynolds number," J. Fluid Mech. **177**, 133–166 (1987).
[18] L. Davidson and S. H. Peng, "Hybrid LES-RANS: A one-equation SGS model combined with a $k-\omega$ model for predicting recirculating flows," Int. J. Numer. Fluids **43**, 1003–1018 (2003).
[19] A. Altıntaş and L. Davidson, "Direct numerical simulation analysis of spanwise oscillating Lorentz force in turbulent channel flow at low Reynolds number," Acta Mech. **228**, 1269–1286 (2017).

28 February 2024 08:49:05

© Author(s) 2024

[20]M. Lee and R. D. Moser, "Direct numerical simulation of turbulent channel flow up to $Re_\tau \approx 5200$," J. Fluid Mech. **774**, 395–415 (2015).
[21]H. Choi, P. Moin, and J. Kim, "Active turbulence control for drag reduction in wall-bounded flows," J. Fluid Mech. **262**, 75–110 (1994).
[22]J. M. Wallace, "Quadrant analysis in turbulence research: History and evolution," Annu. Rev. Fluid Mech. **48**, 131–158 (2016).
[23]J. M. Hamilton, J. Kim, and F. Waleffe, "Regeneration mechanism of near-wall turbulence structures," J. Fluid Mech. **287**, 317–348 (1995).
[24]R. D. Moser and P. Moin, "Direct numerical simulation of curved turbulent channel flow," Technical Report No. 85974 (NASA, 1997).
[25]J. Kim, "On the structure of wall-bounded turbulent flows," Phys. Fluids **26**, 2088–2097 (1983).
[26]H. T. Kim, S. J. Kline, and W. C. Reynolds, "The production of turbulence near a smooth wall in a turbulent boundary layer," J. Fluid Mech. **50**, 133–160 (1971).
[27]Y. Du, V. Symeonidis, and G. E. Karniadakis, "Drag reduction in wall-bounded turbulence via a transverse travelling wave," J. Fluid Mech. **457**, 1–34 (2002).
[28]W. Schoppa and F. Hussain, "Genesis and dynamics of coherent structures in near-wall turbulence," in *Self-Sustaining Mechanisms of Wall Turbulence*, edited by R. Panton (Computational Mechanics Publications, 1997), p. 385.
[29]W. Schoppa and F. Hussain, "Coherent structure dynamics in near-wall turbulence," Fluid Dyn. Res. **26**, 119–139 (2000).
[30]J. Jeong, F. Hussain, W. Schoppa, and J. Kim, "Coherent structures near the wall in a turbulent channel flow," J. Fluid Mech. **332**, 185–214 (1997).
[31]J. Kim and P. Moin, "The structure of the vorticity field in turbulent channel flow. Part 2. Study of ensemble-averaged fields," J. Fluid Mech. **162**, 339–363 (1986).
[32]J. C. R. Hunt, A. A. Wray, and P. Moin, "Eddies, streams, and convergence zones in turbulent flows," in Studying turbulence using numerical simulation databases-II, Proceedings of the 1988 Summer Program, 1988.

28 February 2024 08:49:05

© Author(s) 2024